Inelastic collisions of 2–800-eV He^+ and He_2^+ with Mg and Zn atoms

G. D. Myers and J. J. Leventhal
Department of Physics, University of Missouri-Saint Louis, Saint Louis, Missouri 63121
(Received 21 March 1978)

Inelastic processes leading to excited-state formation have been studied by spectral analysis of collision-produced uv–visible-near-ir radiation for (2–800 eV) He^+ and He_2^+ collisions with Mg and Zn atoms. Although observation of Mg II radiation must result from exothermic charge transfer in the He^+-Mg system, the emission cross sections for the two observed Mg II lines exhibit threshold behavior; it is suggested that production of ground-state Mg III dominates at low energy. He_2^+-Mg collisions yield two prominent Mg II lines, the emission cross sections for which are relatively large at low energy and decrease rapidly with increasing kinetic energy. He^+-Zn collisions produce rich spectra of Zn II lines at all energies and He I lines at elevated energies. In contrast, He_2^+-Zn collisions yield only a few lines with large cross sections at low energy.

I. INTRODUCTION

Since the development of the first gas laser early in the last decade a great deal of effort has been expended in producing new laser transitions in gaseous discharges. In addition to the many laser transitions obtained from gases, there are now a large number that have been achieved using elemental-metal vapors.[1] Most of these transitions involve states of metal ions which have been produced in discharges in He-metal vapor mixtures. For this reason the principal pumping mechanisms are usually charge transfer or Penning ionization involving reactant He^+ and He metastable atoms respectively. Within the last few years a new class of lasers operating with helium partial pressures of the order of atmospheres has led to consideration of the helium dimer ion He_2^+ as an important reactant species.[2-4] This is so because in such high-pressure discharges He_2^+ is the dominant ion.[5]

Both He^+ and He_2^+ have recombination energies (RE) sufficiently high to both ionize and excite many neutral species in charge-transfer excitation processes (CTE). The RE of He^+ is 24.6 eV while the RE of He_2^+ is continuously variable over the approximate range 18.3–20.3 eV,[6] so that efficient CTE is energetically possible with many neutral reactants, including most metal atoms, without the necessity of providing kinetic energy to drive the reaction. We have begun a study of inelastic processes involving helium ions and metal atoms in an effort to better understand known pumping mechanisms, as well as to provide data that may be useful for further laser development.

Our experiments are performed with a mass-selected ion beam and low target-atom densities so that single-collision processes involving well-defined reactants and reactant kinetic energy can be studied. Spectroscopic analysis of collision-produced radiation then provides detailed information on energy partitioning among accessible states of the collision products. In this paper we report studies of inelastic collisions of He^+ and He_2^+ ions with Mg and Zn reactant atoms. Charge-transfer excitation processes are the dominant observed inelastic channel over the energy range studied (2–800 eV). While several CTE-pumped laser transitions have been achieved on Zn II states, none of the Mg II laser transitions are believed to be pumped by charge transfer. Our results suggest that an alternate inelastic channel dominates He^+-Mg collisions at low kinetic energy.

II. EXPERIMENTAL

Data were obtained using a new apparatus designed for study of ion–metal-atom systems at laboratory kinetic energies down to ~2eV. Ions are formed in an electron-impact source, focused into a beam, and accelerated by a set of cylindrical electrostatic lenses. After magnetic mass selection the beam is decelerated to the desired collision energy by another set of electrostatic lenses prior to entering a collision cell. Metal atoms are admitted to the cell from a small cylindrical ceramic oven located under the cell. The atom density is estimated to be ~10^{12} cm^{-3}, which is low enough to ensure single-collision conditions. Several hours were required to stabilize the atom density, as determined by monitoring one of the emission lines.

A fraction of the photons resulting from decay of excited collision products exit the collision cell

through a slot oriented parallel to the ion beam. These photons are then focused on the entrance slit of a Jarrell-Ash 0.25-m scanning monochromator and detector by counting output pulses from a cooled photomultiplier tube. Apparatus control and data acquisition were effected by a microprocessor-based computer. The computer also corrected the collision-produced spectra for the known (absolute) spectral efficiency of the optical system; the efficiency was determined with standard lamps.

The nominal wavelength range of the system is 200–850 nm; however, blackbody radiation from the oven reduced the long-wavelength limit to 760 nm for Zn and 600 nm for Mg. When appropriate, filters were used to suppress second order.

Because the collision cell is cooler than the oven, it is difficult to accurately establish the metal-atom density in the cell. This makes determination of absolute cross sections correspondingly difficult. It is possible to estimate the Zn-atom density from the He^+-Zn 589 nm Zn II emission cross sections reported by Soskida and Shevera,[7] using our apparatus geometry, optical efficiency, and measured ion beam and 589-nm signals. As stated above, this procedure yields a density of $\sim 10^{12}$ cm^{-3}. The absence of beam attenuation when the oven was heated suggests that this density is not unreasonable. Using gaseous targets, for which atom (or molecule) densities can be determined using a capacitance manometer, beam attenuation is usually observed when the density is $\sim 10^{13}$ cm^{-3}. Because details of the absolute measurements reported in Ref. 7 are not given, we have elected to display relative rather than absolute cross sections. However, it should be noted that the kinetic-energy dependence of this emission cross section is in qualitative agreement with the earlier measurement.

By correlating the measured oven temperature with the estimated Zn-atom density and comparing the Zn and Mg vapor-pressure curves,[8] an oven temperature corresponding to a Mg-atom density of $\sim 10^{12}$cm^{-3} was estimated; the oven was operated at this temperature. Using this crude technique it is possible to relate the Mg cross sections to the Zn cross sections so that the "arbitrary units" on all cross-section graphs may be considered to be the same, within the limits of the above technique. We have arranged the scales so that if the atom densities are 10^{12} cm^{-3}, one arbitrary unit corresponds to a cross section of 1 Å^2.

III. RESULTS

A. Magnesium

Emissions observed from collisions of He^+ and He_2^+ ions with Mg atoms are indicated in Fig. 1.

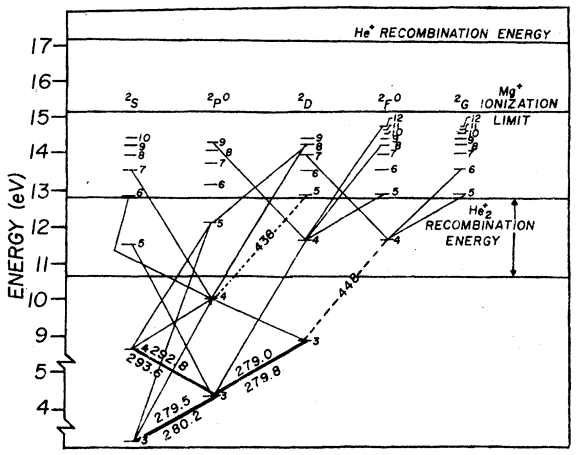

FIG. 1. Partial Grotrian diagram for Mg II. Heavy lines indicate emissions present in both collision-produced spectra; dashed lines indicate emissions produced only from He_2^+-Mg collisions. Energies are relative to the ground state of Mg II and wavelengths are in nanometers.

The transitions observed from impact of each ion are illustrated by the spectra in Fig. 2. For both systems the most prominent spectral feature is at 279 nm and is clearly owing to product Mg^+, but

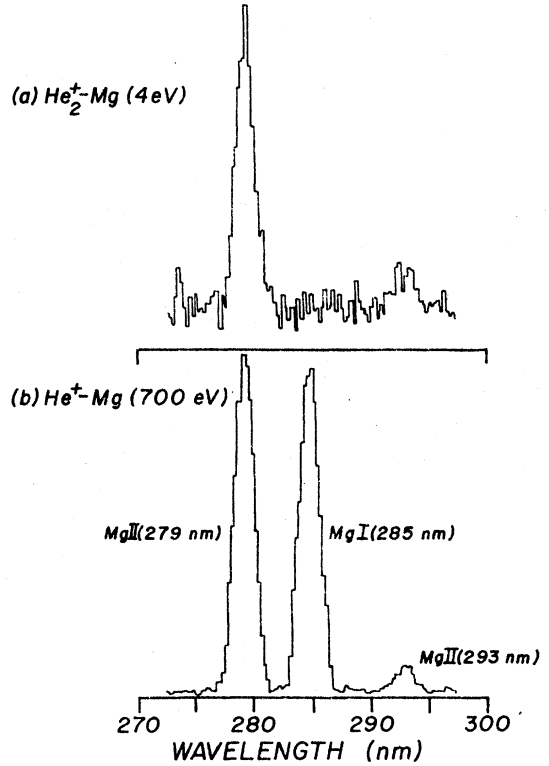

FIG. 2. Emission spectra corrected for spectral efficiency from 4-eV He_2^+-Mg collisions and 700-eV He^+-Mg collisions. The ordinate is proportional to quanta/sec.

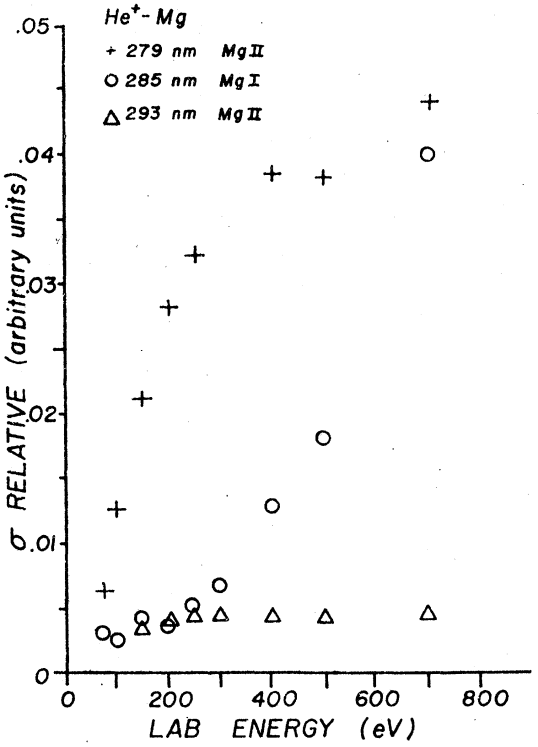

FIG. 3. Emission cross sections for the indicated l lines resulting from He^+-Mg collisions. The ordinate scales are the same for Figs. 3 and 4 and for all cross-section plots to the extent discussed in Sec. II.

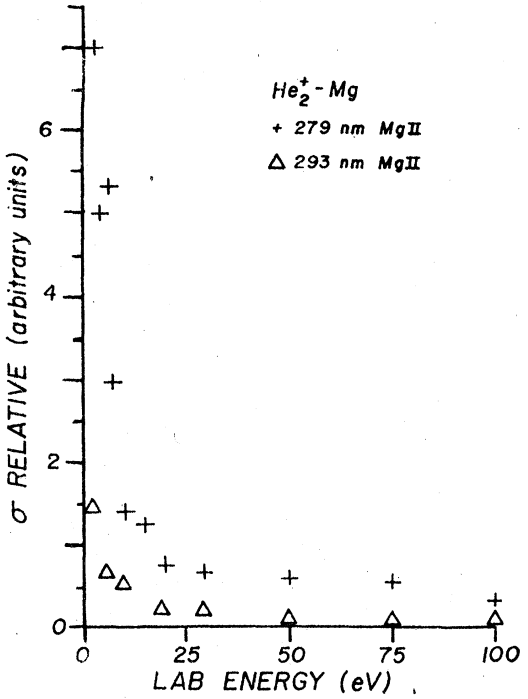

FIG. 4. Emission cross sections for the indicated lines resulting from He_2^+-Mg collisions. The ordinate scales are the same for Figs. 3 and 4 and for all cross-section plots to the extent discussed in Sec. II.

the $3d\,^2D \rightarrow 3p\,^2P^o$ transitions cannot be resolved from the $3p\,^2P^o \rightarrow 3s\,^2S$ transitions. The latter doublet must be a major constituent since the upper state would be populated by cascading if not directly (see Fig. 1). Because of the inability to resolve the two transitions that radiate at 279 nm it is impossible to determine which of the two upper states is formed in the ion-atom collisions. Since production of the $3d\,^2D$ is less exothermic (by ~4.4 eV), it might be inferred that this state is preferred. Previous work indicates that this may not necessarily be the case.[9]

A major difference between the He^+ and He_2^+ collision systems is the observation of Mg I 285-nm resonance radiation from He^+-Mg collisions. Only Mg II radiation is observed from He_2^+-Mg collisions. The kinetic-energy dependence of the Mg I 285-nm resonance radiation emission cross section is shown in Fig. 3 along with the relative cross sections for production of 279 and 293-nm radiation. Except for some He I lines observed at kinetic energies above ~300 eV (such as the 587.5-nm $3d\,^3D \rightarrow 2p\,^3P^o$ transition) these are the only observed spectral features resulting from 2–700-eV He^+-Mg collisions. It is interesting that although the observed Mg II radiation results from exothermic charge-transfer processes, the kinetic-energy dependence exhibits threshold behavior of the type characteristic of endothermic processes. Production of Mg I ($3p\,^2P^o$), which yields the 285-nm resonance radiation, is of course an endothermic collision-induced excitation (CIE) process. Although the cross section for this CIE process exhibits threshold behavior, the steep rise does not occur until nearly 300 eV of kinetic energy is available for conversion into internal energy.

As noted above only Mg II radiation has been detected from He_2^+-Mg collisions, even at elevated kinetic energies. The strongest emissions are the same as the observed Mg II radiation from He^+-Mg collisions, 279 and 293 nm, as shown in Fig. 2. The background signal for He_2^+-Mg collisions is relatively higher because the He_2^+ beam current is lower than that of He^+ by three orders of magnitude. Weaker Mg II lines were observed at 438 and 448 nm; both of these transitions originate in states that lie within the He_2^+ RE band. With the exception of the $5p\,^2P^o \rightarrow 3d\,^2D$ transitions at 385 nm, no other transition from states lying within the He_2^+ RE band are accessible with the present apparatus.

Figure 4 shows the cross-section behavior of the 279 and 293-nm radiation a function of collision kinetic energy for the He_2^+-Mg system. In contrast

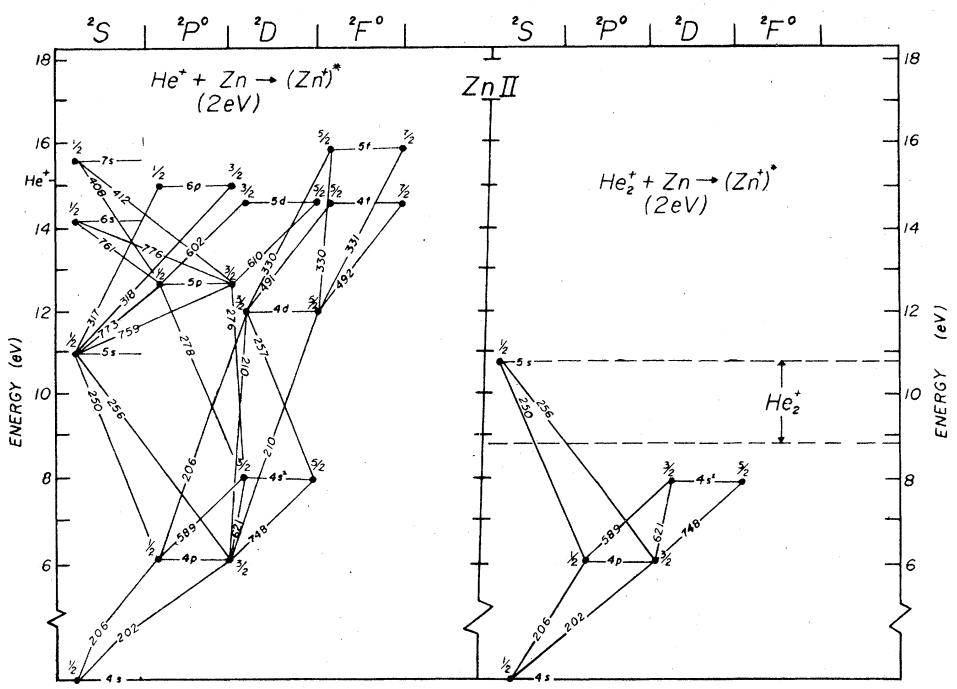

FIG. 5. Partial Grotrian diagrams for Zn II showing transitions observed from 2-eV He^+-Zn and He_2^+-Zn collisions. Energies are relative to the ground state of Zn II and wavelengths are in nanometers.

to the He^+-Mg CTE cross sections, the behavior is characteristic of exothermic or thermoneutral processes; that is, the cross section increases with decreasing collision energy. Note that these cross sections are considerably higher than those observed for the He^+-Mg system.

B. Zinc

The Zn II transitions observed from 2-eV He^+-Zn and 2-eV He_2^+-Zn collisions are shown in Grotrian diagrams in Fig. 5. In contrast to He^+-Mg collisions, the He^+-Zn collisions yield rich spectra.

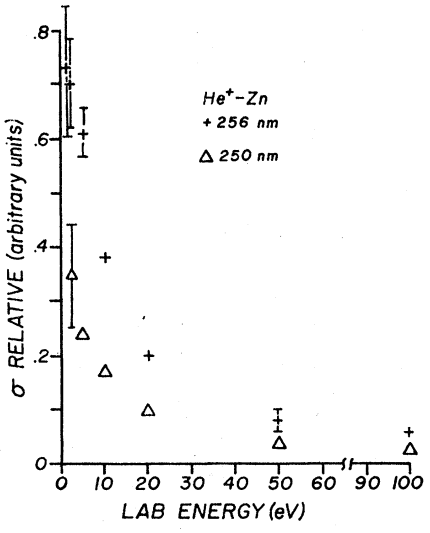

FIG. 6. Emission cross sections for the indicated Zn II lines resulting from He^+-Zn Collisions. The ordinate scales are the same for Figs. 6–8 and 11 and for all cross-section plots to the extent discussed in Sec. II.

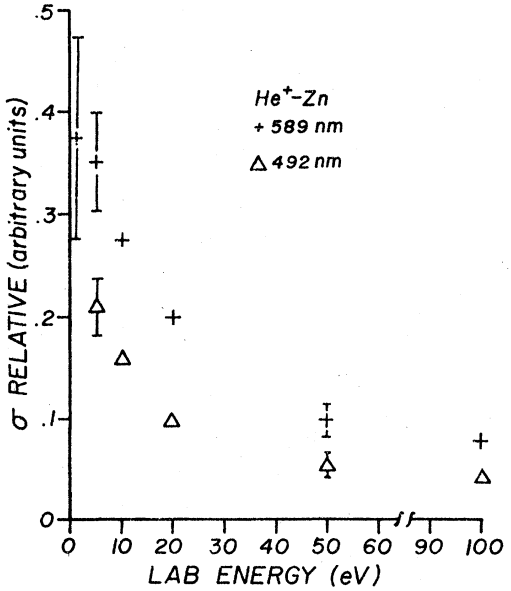

FIG. 7. Emission cross sections for the indicated Zn II lines resulting from He^+-Zn collisions. The ordinate scales are the same for Figs. 6–8 and 11 and for all cross-section plots to the extent discussed in Sec. II.

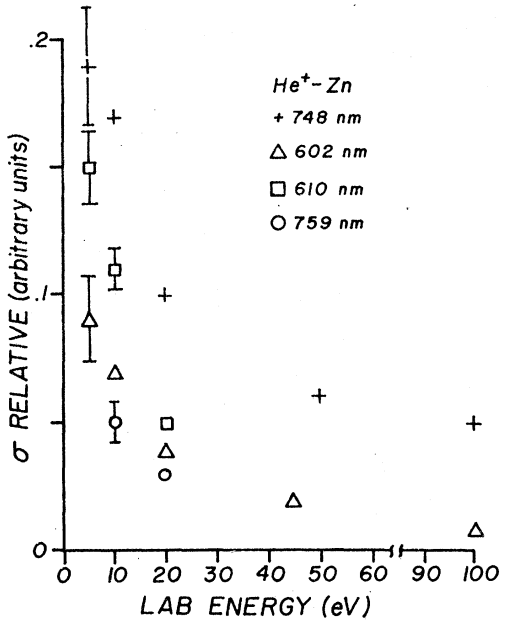

FIG. 8. Emission cross sections for the indicated Zn II resulting from He^+-Zn collisions. The ordinate scales are the same for Figs. 6–8 and 11 for all cross-section plots to the extent discussed in Sec. II.

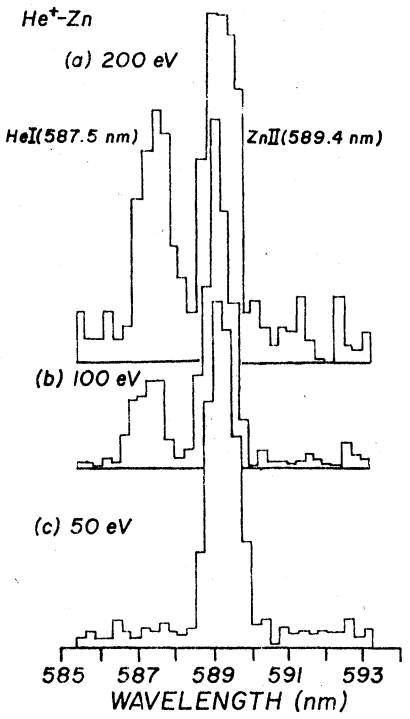

FIG. 9. Emission spectra from He^+-Zn collisions at three different laboratory kinetic energies illustrating the emergence of the He I line at 587.5 nm with increasing kinetic energy. The ordinate is proportional to quanta/sec.

Figures 6–8 show relative emission cross sections for the strongest lines; the behavior is characteristic of exothermic processes. As the collision energy was increased, several He I lines, resulting from (endothermic) electron capture by He^+, were observed. The appearance of this process with increasing kinetic energy, which was also observed in the He^+-Mg system, is illustrated in Fig. 9 which shows the 587.5-nm He I line emerging near the 589-nm Zn II line.

The selectivity of He_2^+-Zn CTE process as compared to the He^+-Zn system is illustrated in Fig. 5. No emissions originating in states higher than the He_2^+ RE band were observed. This selectivity is further illustrated in Fig. 10 which shows 4-eV He^+-Zn and He_2^+-Zn spectra. The apparently higher background count level in the He_2^+ case is again owing to lower beam current. Figure 11 shows emission cross sections for three lines resulting from He_2^+-Zn collisions. The 748-nm line, which is part of the same multiplet as the 589-nm line, was not studied in detail because blackbody radiation from the oven produced relatively high background count levels in the accessible infrared region of the spectrum.

IV. DISCUSSION

The He^+-Mg system is an interesting one because the sum of the first two ionization potentials of magnesium is less than the first ionization poten-

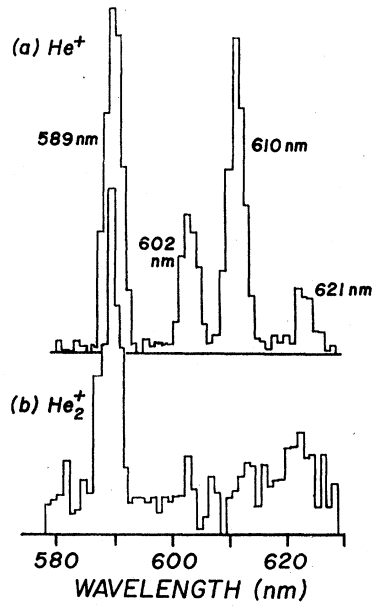

FIG. 10 Emission spectra from 4-eV He^+-Zn and He_2^+-Zn collisions, corrected for spectral efficiency. The ordinate is proportional to quanta/sec.

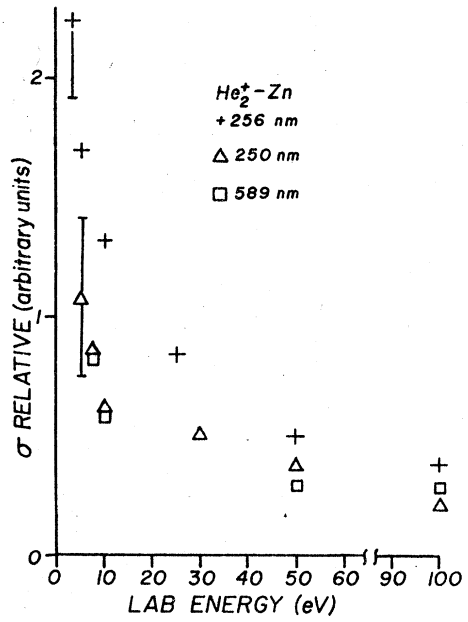

FIG. 11. Emission cross sections for the indicated Zn II lines resulting from He_2^+-Zn collisions. The ordinate scales are the same for Figs. 6–8 and 11 and for all cross-section plots to the extent discussed in Sec. II.

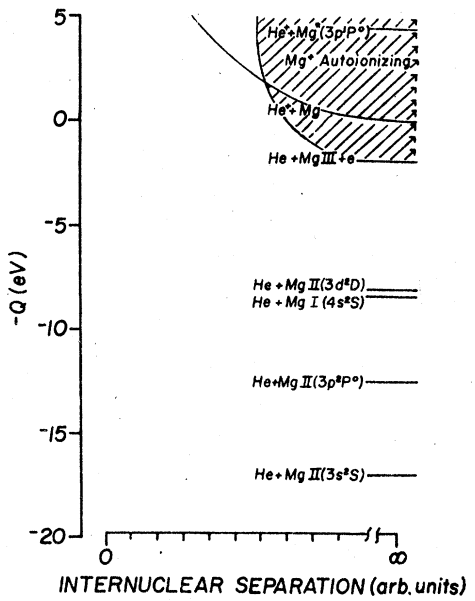

FIG. 12. Energy-level diagram for various states of $(He\text{-}Mg)^+$ at infinite separation. The ordinate shows the difference between initial and final relative kinetic energies, Q, for production of these final states from ground-state He^+-Mg collisions. Also shown are schematic potential-energy curves for ground state He^+-Mg and $He\text{-}Mg^{++}$- e as described in the text. The cross-hatched portion represents the continuum of states available to the $He\text{-}Mg^{++}$- e system.

tial of helium. Therefore the reaction

$$He^+ + Mg \rightarrow Mg^{++} + He + e \qquad (1)$$

is exothermic (by about 1.9 eV). Figure 12 is an energy-level diagram together with qualitative sketches of possible potential-energy curves for various combinations of $(He\text{-}Mg)^+$. At infinite separation He^+-Mg lies about 1.9 eV above the lowest energy $He\text{-}Mg^{++}$-e channel; since the electron can have any kinetic energy, there exists a continuum of states available to the system in the $He\text{-}Mg^{++}$-e exit channel. For the purpose of illustration we have shown the lowest $He\text{-}Mg^{++}$ potential energy to be repulsive. The He^+ $(1s\ ^2S)$-$Mg(3s\ ^1S)$ potential is also shown to be repulsive as has been suggested by Kulander and Dahler.[11] At low He^+-Mg kinetic energy it seems likely that the system will switch to one of the continuum $(He\text{-}Mg^{++}\text{-}e)$ states. Efficient production of Mg^{++} in thermal energy He^+-Mg collisions has been observed[12]; presumably the Mg^{++} results from reaction (1). As the kinetic energy increases the system is more likely to pass through the continuum and thus open additional exit channels. For example when the He^+-Mg internuclear separation is such that the system is no longer imbedded in the $He\text{-}Mg^{++}$ continuum, it is possible to access a crossing with the He^+-$Mg(3p\ ^1P^o)$ curve (not shown in Fig. 12). If this occurs it can lead to the observation of 285-nm radiation. The data are consistent with such a picture since all three prominent spectral features exhibit threshold behavior (see Fig. 3) suggesting that kinetic energy must be supplied to drive the reaction. This is a different picture than that usually envisioned for threshold-type processes. In the present case, if our suggestion is correct, kinetic energy is required so that the system can pass through the continuum; usually kinetic energy is required to overcome an activation energy or drive an endothermic process.

It is interesting that of the relatively few known laser transitions from Mg II states, none are believed to be pumped by He^+-Mg charge transfer. This is in contrast to a variety of other elemental metals such as zinc, cadmium, selenium, and tellurium.[1] The inability of He^+-Mg to produce inverted Mg II state populations in thermal energy discharges is consistent with the suggestion that production of Mg^{++} is preferred at low relative energies.

As noted in Sec. III the only reaction channels observed for He_2^+-Mg collisions are exothermic or thermoneutral CTE channels with excited product Mg^+. Furthermore, the behavior of the emission cross sections as a function of collision energy is characteristic of exothermic or thermoneutral processes (see Fig. 9). The He_2^+-Mg results show

no preference for formation of production states which lie within or very near the He_2^+ RE band. This is in contrast to earlier He_2^+ CTE studies from our laboratory[10] as well as the He_2^+-Zn results reported here (see Figs. 5 and 10). The failure to detect selective population of Mg^+ states lying within the He_2^+ RE band may be a consequence of branching ratios which favor radiation from these states at wavelengths inaccessible with our present apparatus, or in some cases, the states may not radiate at any wavelength within our detectable range. An example of a state in the latter category is the Mg II ($5s\ ^2S$) state which radiates as shown:

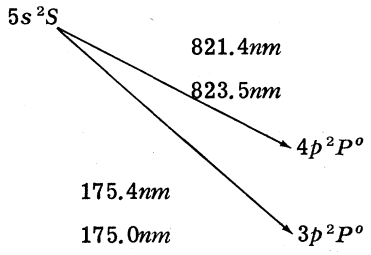

The doublet at 175 nm is the strongest pair of lines in the discharge spectrum of Mg II, while the 821–823-nm doublet is of comparable intensity to the next strongest.[13] Thus the $5s\ ^2S$ state of Mg II radiates strongly, but unfortunately is not detectable in these experiments.

The He^+-Zn and He_2^+-Zn results obtained in these experiments are in many ways similar to the analogous Cd studies reported earlier.[10] This is not surprising since zinc and cadmium, which are both group IIb elements, have similar chemical properties. Low-energy He^+ impact yields a rich spectrum for both Zn and Cd, while He_2^+ collisions are considerably more selective in producing excited Zn II and Cd II states. For He_2^+-Cd collisions, the $4d^9 5s\ ^2D$ Cd II states were selectively populated; these states are formed by removing a single $4d$ electron from Cd I [electron configuration: $(4d)^{10}(5s)^2$]. For He_2^+-Zn collisions the analogous $3d^9 4s^2\ ^2D$ states are also formed (by removal of a single $3d$ electron from Zn I), however, in this case production of the Zn II $5s\ ^2S$ state is comparable. Previous results[10,14] suggest that CTE processes in which only a single electron is removed may be favored over processes which require removal of one electron and promotion of a remaining electron. In the present case, however, formation of Zn II $5s\ ^2S$ state by a two-electron process competes favorably with the one-electron processes. Since both the $5s\ ^2S$ and $4s^2\ ^2D$ states radiate to the $4p\ ^2P^o$ state of Zn II it appears as if population inversion on either of these states might be difficult to achieve under circumstances in which He_2^+ is the dominant ionic species. Although laser transitions at 589 and 748 nm have been produced the pumping mechanism was Penning ionization rather than charge transfer.[1]

ACKNOWLEDGMENTS

This research was supported by the Office of Naval Research under Contract No. N00014-76-C-0760. The authors would like to thank Dr. B. R. Junker for helpful discussions.

[1]See, for example: (a) C. C. Davis and T. A. King, in *Advances in Quantum Electronics*, edited by D. W. Goodwin (Academic, New York, 1975), Vol. 3 p. 170; (b) C. S. Willet, *Introduction to Gas Lasers: Population Inversion Mechanisms* (Pergamon, New York, 1974).

[2]C. B. Collins and A. J. Cunningham, Appl. Phys. Lett. 27, 127 (1975); C. B. Collins, A. J. Cunningham, and M. Stockton, Appl. Phys. Lett. 25, 344 (1974); R. A. Waller, C. B. Collins, and A. J. Cunningham, Appl. Phys. Lett. 27, 323 (1975).

[3]J. B. Laudenslager, T. J. Pacala, and C. Wittig, Appl. Phys. Lett. 29, 580 (1976).

[4]D. E. Rothe and K. O. Tan, Appl. Phys. Lett. 30, 152 (1977).

[5]R. Deloche, P. Monchicourt, M. Cheret, and F. Lambert, Phys. Rev. A 13, 1140 (1976).

[6]J. J. Leventhal, J. D. Earl, and H. H. Harris, Phys. Rev. Lett. 35, 719 (1975).

[7]M.-T. I. Soskida and V. S. Sherera, JETP Lett. 22, 269 (1975).

[8]F. Rosebury, *Handbook of Electron Tube and Vacuum Techniques* (Addison-Wesley, New York, 1965).

[9]See, for example, (a) R. E. Olsen and F. T. Smith, Phys. Rev. A 7, 1529 (1973); (b) H. H. Harris, M. G. Crowley, and J. J. Leventhal, Chem. Phys. Lett. 29, 540 (1974).

[10]F. Ranjbar, H. H. Harris, and J. J. Leventhal, Appl. Phys. Lett. 31, 385 (1977), and references cited therein.

[11]K. C. Kulander and J. S. Dahler, J. Phys. B 8, 2679 (1975).

[12](a) E. L. Latush and M. F. Sem, Pis'ma Zh. Eksp. Teor. Fiz. 15, 645 (1972) [JETP Lett. 15, 457 (1972)]; (b) R. Arrathoon, I. M. Littlewood, and C. E. Webb, Phys. Rev. Lett. 31, 1168 (1973); (c) V. V. Zhukov, E. L. Latush, and M. F. Sem, Sov. Phys. J. 20, 957 (1977).

[13]A. R. Striganov and N. S. Sventitaskii, *Tables of Spectral Lines of Neutral and Ionized Atoms* (Plenum, New York, 1968).

[14]G. H. Bearman and J. J. Leventhal, Phys. Rev. A (to be published).